

# RSC Advances



This is an *Accepted Manuscript*, which has been through the Royal Society of Chemistry peer review process and has been accepted for publication.

*Accepted Manuscripts* are published online shortly after acceptance, before technical editing, formatting and proof reading. Using this free service, authors can make their results available to the community, in citable form, before we publish the edited article. This *Accepted Manuscript* will be replaced by the edited, formatted and paginated article as soon as this is available.

You can find more information about *Accepted Manuscripts* in the [Information for Authors](#).

Please note that technical editing may introduce minor changes to the text and/or graphics, which may alter content. The journal's standard [Terms & Conditions](#) and the [Ethical guidelines](#) still apply. In no event shall the Royal Society of Chemistry be held responsible for any errors or omissions in this *Accepted Manuscript* or any consequences arising from the use of any information it contains.

# The electrocatalytic activity of IrO<sub>2</sub>-Ta<sub>2</sub>O<sub>5</sub> anode materials and Electrolyzed Oxidizing Water preparation and sterilization effect

Zhandong Ren\*, Shanshan Quan, Jie Gao, Wenyang Li, Yuchan Zhu\*,

Ye Liu, Bo Chai, Yourong Wang

(School of Chemical and Environmental Engineering, Wuhan Polytechnic University, Wuhan, 430023, China)

**Abstract:** Ti/IrO<sub>2</sub>-Ta<sub>2</sub>O<sub>5</sub> anode electrocatalysts with different content and temperature were prepared with thermal decomposition in this work. The crystallite characterization and the morphology were examined via XRD and SEM. The electrochemical properties were examined via cyclic voltammetry (CV) in 0.5M H<sub>2</sub>SO<sub>4</sub> and linear sweep voltammetry (LSV) in saturated sodium chloride. Through the study of different series of Ti/IrO<sub>2</sub>-Ta<sub>2</sub>O<sub>5</sub> anodes, we can find that the preparation conditions have a great impact on the electrode catalytic activity. The experimental results indicate that that the electrochemically active surface area is determined by the content and morphology of the anode coating. When the IrO<sub>2</sub> content and the preparation temperature is 70% and 500°C, the surface of electrode is aggregated with the segregated crystallite particle like flower, which brings about the best electrode catalytic activity. The activity of chlorine evolution reaction of IrO<sub>2</sub>-Ta<sub>2</sub>O<sub>5</sub> (70% and 500°C) is 0.4A·cm<sup>-2</sup> in saturated sodium chloride. The properties and sterilization effect of EO water is closely related to the electrode catalytic activity. The higher the current of chlorine evolution is, the higher the available chlorine and HClO content is. When the IrO<sub>2</sub> content is 70% and the preparation

temperature is 500°C, the maximum value of Killing logarithm value and killing rate is 3.01-3.05 and 99.9023-99.9109% respectively. In addition, when the Ti substrate was dealt with 40 minutes of activation treatment, the Ti/IrO<sub>2</sub>-Ta<sub>2</sub>O<sub>5</sub> anodes have the best stability.

**Keywords:** Ti/IrO<sub>2</sub>-Ta<sub>2</sub>O<sub>5</sub>, Chlorine Evolution, Electrolyzed Oxidizing Water, Sterilization Effect

## 1. Introduction

The disease caused by food is widespread throughout the world. Foodborne diseases are the most prominent health problems in the world, which is directly related to people's life safety and health. Therefore, the new food sterilization technology which has a wide adaptability, high efficiency, broad spectrum, safety and no residual is very important for food industry. Electrolyzed oxidizing water (EO water), with low pH (2.2-2.7), high oxidation-reduction potential (ORP, >1100mV), and available chlorine content of 30 to 80 mg·L<sup>-1</sup>, which has high bactericidal activity and wide adaptability against many foodborne pathogens<sup>[1]</sup>. EO water has been designated as food fungicide in Japan<sup>[2]</sup> and has the strong sterilization ability for agricultural products, including lettuce<sup>[3]</sup> (*Escherichia coli*); carrot<sup>[4]</sup> (*Aerobic Bacteria, Molds, Yeasts*); fish<sup>[5]</sup> (*Listeria monocytogenes, Morganella morganiion*); shrimp<sup>[6]</sup> (*Vibrio parahaemolyticus*); pork<sup>[7-9]</sup> (*Escherichia coli, Listeria monocytogenes*); egg<sup>[10]</sup> (*Salmonella enteritidis*); apple<sup>[11]</sup> (*Escherichia coli, Listeria innocuaor, Salmonella choleraesuis*); peanut<sup>[12]</sup> (*aflatoxin B1*) and cabbage<sup>[2]</sup> (*Escherichia coli*). In addition, several studies have shown that EO water can be effective in killing fungus (*Candida spp.; Aspergillus spp.*), blood virus (*Hepatitis B virus; hepatitis C virus; human immunodeficiency virus*) and toxin (*Staphylococcal enterotoxin-A; Aspergillus parastiticus aflatixin*)<sup>[1]</sup>. When it comes to the sterilization mechanism of EO water, there are two main theories, one is the physics (high ORP and low pH)<sup>[13-19]</sup>, the other is the chemical theory (available chlorine concentration and active oxygen)<sup>[20-25]</sup>. Nevertheless, there is no definite conclusion about the disinfection targets of EO water for lack of authentic evidences on molecular biological level.

EO water is generated by electrolysis of a dilute salt (NaCl) solution in an electrolysis

chamber where anode and cathode electrodes are separated by a membrane. In 2005, Hsu first explored the influence of velocity, salinity and temperature on the preparation of EO water<sup>[26-27]</sup>. However, little information concerning preparation of electrode material had been investigated until now<sup>[28]</sup>. For example, the commercial electrode material was still dominated by platinum for a long time because of its electrolysis stability. But the performance of chlorine evolution of platinum is very poor compared with that of ruthenium (see table S1 and literature 29). Ruthenium has good activity not only for chlorine evolution in saturated sodium chloride solution used in chlor-alkali industry<sup>[29-35]</sup>, but also for oxygen evolution in sulfuric acid or sodium sulfate solution<sup>[36-41]</sup>. It should be noted that the chloride concentration (0.05wt%) in the EO water's preparation is much lower than its in chlor-alkali industry. So a large quantities of oxygen evolution reaction would be proceed in the electrolysis process of EO water's preparation, which may result in a low current efficiency. It would destroy the hypoxia solid solution's structure of the oxide electrode's surface, resulting in the reduction of electrolysis efficiency and lifetime of the electrode<sup>[42-46]</sup>. Iridium has a stable structure in acid medium and can effectively catalyze the oxygen evolution reaction<sup>[33,34,46-52]</sup>. But there are a few literatures about the chlorine evolution reaction of IrO<sub>2</sub> electrode<sup>[47,53-54]</sup>, the activity of chlorine evolution reaction on iridium is also poor in contrast to ruthenium (see table S1). So the activity of chlorine evolution reaction on iridium should be further enhanced and it is very important for EO water's preparation. It would enhance the activity of chlorine evolution reaction of electrode through alloying with other metals<sup>[28]</sup>.

In this work, IrO<sub>2</sub>-Ta<sub>2</sub>O<sub>5</sub> electrocatalysts with different contents and temperature were prepared with thermal decomposition. The XRD, SEM and XRF characterizations were

employed to study the performance of the IrO<sub>2</sub>-Ta<sub>2</sub>O<sub>5</sub>. The relationship between the physicochemical property of IrO<sub>2</sub>-Ta<sub>2</sub>O<sub>5</sub> electrode and electrochemical behavior was established through the cyclic voltammograms(CV) and chlorine evolution reaction(CER). Furthermore, the values of pH, ORP, ACC and sterilization effect of EO water using a series of IrO<sub>2</sub>-Ta<sub>2</sub>O<sub>5</sub> electrodes(different compositions and temperatures) as anode materials had been systematically discussed in this article. In addition, the stabilities of IrO<sub>2</sub>-Ta<sub>2</sub>O<sub>5</sub> electrodes with different activating treatment times of Ti substrate were also investigated for its further industrial application.

## 2. Materials and Methods

### 2.1 Electrode preparation

The titanium plate of Grade TA1(1cm×1cm) was utilized as the electrode substrate, which was sand-blasted, degreased in acetone and then in the boiling 10% oxalic acid at 96°C for 2h to produce gray surface with uniform roughness. The preparation of the titanium based IrO<sub>2</sub>-Ta<sub>2</sub>O<sub>5</sub> coatings anode for conventional method of thermal decomposition was described elsewhere in detail<sup>[33,47,55-57]</sup>. The precursors H<sub>2</sub>IrCl<sub>6</sub> and TaCl<sub>5</sub> were dissolved in 1:1 volume ratio isopropanol and ethanol mixed solutions, in which the total metal concentration was kept at around 0.2mol·L<sup>-1</sup>. When the mole ratio of H<sub>2</sub>IrCl<sub>6</sub> and TaCl<sub>5</sub> were 1:18, 4:12, 6:8, 7:6 and 9:2, titanium-based IrO<sub>2</sub>-Ta<sub>2</sub>O<sub>5</sub> coated anodes with a nominal content of 10%, 40%, 60%, 70% and 90% IrO<sub>2</sub> would be obtained. The precursors were applied to the pretreated titanium substrate with a brush, which were dried at 100°C for 10min in the oven, and then sintered in the furnace at 500°C for 10min. The above steps were repeated 10 times, with the total oxides loading of about 1.5mg·cm<sup>-2</sup>, after which the samples were heated at the same annealing temperature for

1h.

## 2.2 Material characterization

X-ray diffraction (XRD) was used to analyze the structure of electrode coating. The inspection was carried out at room temperature on a D/Max-III A diffractometer (Rigaku, Japan), using  $\text{Cu K}_\alpha$  radiation operating at 40kV and 30mA. The surface morphology of the oxide electrode was characterized by scanning electron microscopy (SEM: S-3000N, Hitachi Co., Japan). The analysis of the composition of the electrode was characterized by X-ray Fluorescence (XRF: EDX-720, Shimadzu, Japan).

## 2.3 Electrochemical measurement

All of the electrochemical measurements were carried out in a typical three-electrode electrochemical glass cell. A platinum plate was used as the counter electrode, and KCl saturated calomel electrode (SCE) as the reference. Cyclic voltammetry (CV) measurements were performed in  $0.5\text{mol}\cdot\text{L}^{-1}$   $\text{H}_2\text{SO}_4$  solution at  $25^\circ\text{C}$  with a CHI760D potentiostat. Linear sweep voltammetry measurements were performed in saturated NaCl solution. Accelerated electrolysis life tests were carried out under the condition of  $0.5\text{mol}\cdot\text{L}^{-1}$   $\text{H}_2\text{SO}_4$  solution,  $2\text{A}\cdot\text{cm}^{-2}$  of anodic current density, Ti plate as a counter electrode and the temperature  $40^\circ\text{C}$ . As for electrochemical tests, the surface of the specimen was covered with epoxy resin except for the working area ( $1\text{cm}^2$ ) on one side.

## 2.4 Preparation and analysis of EO water

The generation of EO water involved electrolysis of NaCl in a three-room cell containing inert positively charged and negatively charged electrodes separated by anion membrane and cation membrane shown in Figure 1. The anode is  $\text{IrO}_2\text{-Ta}_2\text{O}_5$ , and the cathode is titanium plate. A salt

solution (0.5wt% NaCl) was pumped into the EO water generator. The current density are  $40\text{mA}\cdot\text{cm}^{-2}$  and  $160\text{mA}\cdot\text{cm}^{-2}$ , and the electrode distance is 2cm. Two types of water possessing different characteristics were generated: electrolyzed oxidizing water ( $\text{pH}<2.6$ ,  $\text{ORP}>1100\text{mV}$ ) containing dilute hypochlorous acid (HOCl) was produced from the anode side with approximately  $20\text{-}200\text{mg}\cdot\text{L}^{-1}$  free chlorine, and electrolyzed reduced water ( $\text{pH}>11$ ,  $\text{ORP}<-795\text{mV}$ ) containing dilute NaOH was produced by the cathode.

The value of pH and ORP were analyzed by pH meter (3-Star, Thermo Orion). The concentration of total active chlorine dissolved in the solution was determined using the TMB (3,3',5,5'-tetramethyl benzidine) colorimetric method. In this method, TMB is oxidized to form a yellow product and its concentration was analyzed immediately using a spectrophotometer (UV-2102PC, UNICO, US) at 450 nm. The content of HClO is measured directly by spectrophotometer at 233 nm, which the absorption coefficient  $\varepsilon$  is  $100^{[58]}$ . They were measured three times and the average values were obtained.

## 2.5 Bactericidal effect of EO water

*Bacillus subtilis var. niger* (ATCC 9372) (purchased from China General Microbiological Culture Collection Center) was employed as an indicator bacterium in all disinfection experiments. The initial populations of *B. subtilis* for each disinfection experiment is approximately  $7.53\text{ lgCFU}\cdot\text{mL}^{-1}$ . During the experiments, 1.0 mL of bacteria suspension was mixed with 9.0mL of EO water in a sterile tube and was immediately quenched with excess  $\text{Na}_2\text{S}_2\text{O}_3$  ( $10\text{ mmol}\cdot\text{L}^{-1}$ ) to eliminate the residual disinfectants in the sample solution after 30min.

The survival of *B. subtilis* was determined by the colony counting method using tryptic soy

agar(TSA) plate with serial dilutions in Butterfield's phosphate buffer (pH 7.2-7.4). To prepare the counting plate, 1mL of each appropriate dilution of *B. subtilis* culture was mixed carefully with 15ml of TSA at 45-47°C, and then transferred into petri dish at ambient temperature for solidification. After completely solidification, an overlay adding 5ml to 10ml VRBL was poured on the surface of the inoculated medium. The plates were incubated at 35°C for 48h and the colonies formed on plates were counted. Significant differences between treatments were established at a significance level of  $p=0.05$ .

### 3. Results and Discussion

#### 3.1 Composition analysis of IrO<sub>2</sub>-Ta<sub>2</sub>O<sub>5</sub>

The actual compositions of the oxide electrodes with different proportion and temperature were examined by XRF, and their results are listed in Table S2. The majority of electrode's actual composition is consistent with nominal composition, such as 60% (450°C), 70% (450°C, 500°C, 550°C, 650°C) and 90% (450°C). But for 10% sample, there is a large deviation between the actual composition and nominal composition. The possible reason is that when the content of TaCl<sub>5</sub> is too high, it will be easy to occur that the hydrolysis of TaCl<sub>5</sub> for its unstable nature and reduce the content of TaCl<sub>5</sub> in a solid solution.

#### 3.2 Effect of IrO<sub>2</sub> content on surface morphology

Since the kinetics of the chlorine evolution reaction is very fast, the main active site is the outer surface. In order to improve the catalytic activity of a chlorine electro-catalyst it is necessary to specifically increase the outer surface area. So the surface morphology plays an important role in the gas-evolving chlorine catalysis reaction. As can be seen from Figure 2, dried-mud cracks

appear in all the samples as a result of sintering process, which is quite typical for oxide electrodes. The reason is the quick volatilization of organic solvents and the stress caused by different coefficients of heat expansions between the substrate and the coatings. But the surface morphologies are different with the IrO<sub>2</sub> content varied in the coating. It can be seen that there are islands separated by wide and deep cracks and a few of crystallite particles in Ti/IrO<sub>2</sub>-Ta<sub>2</sub>O<sub>5</sub> anodes with 10% IrO<sub>2</sub> in Figure 2a. In Figure 2b, it is found that the cracks become less and narrower in comparison with sample in Figure 2a, while there are some large IrO<sub>2</sub> crystallite particles with average sizes about 20-30 nm. As for Ti/IrO<sub>2</sub>-Ta<sub>2</sub>O<sub>5</sub> anodes with 60% and 70% IrO<sub>2</sub> (Figure 2c and Figure 2d), the surface of the anodes are covered by more and more fine crystal particles like flower agglomerates which tend to connect to form networks without cracks. In addition, the film thickness is about 150μm from a cross-section SEM of 70% IrO<sub>2</sub> anode in Figure 2f and the oxide crystals are lined up tightly. However, it is found that the crystallite particles disappeared and dried-mud cracks appeared again in Ti/IrO<sub>2</sub>-Ta<sub>2</sub>O<sub>5</sub> anodes with 90% IrO<sub>2</sub> in Figure 2e, which indicates that the IrO<sub>2</sub> crystallites agglomerates are emerged when the content of IrO<sub>2</sub> is too high. So the existence of proper quantities of Ta<sub>2</sub>O<sub>5</sub> modification in the coating results in a typical morphology of the oxide solid solution, which is provided with dried-mud cracks, networks and fine crystal particles.

The deduction has been confirmed by XRD curves as shown in Figure 3. The resulting peak positions and intensities were compared with the JCPDS reference files for IrO<sub>2</sub> (No.15-870), Ta<sub>2</sub>O<sub>5</sub> (No.25-0922) and Ti(No.44-1294). There is no evidently diffraction peak of Ta<sub>2</sub>O<sub>5</sub> in all XRD curves except 10% IrO<sub>2</sub>, which indicates that the crystallization of Ta<sub>2</sub>O<sub>5</sub> is restrained by the existence of IrO<sub>2</sub>. The obvious diffraction peaks of β-Ta<sub>2</sub>O<sub>5</sub>(22.8°, 28.7°, 36.8°)

only appear in 10% IrO<sub>2</sub> coating, although their intensities are not much strong. IrO<sub>2</sub> rutile began to appear in 40% IrO<sub>2</sub> films and the peaks of β-Ta<sub>2</sub>O<sub>5</sub> had disappeared. As IrO<sub>2</sub> content is up to 60%, the crystallite phase in the mixture exists entirely as rutile phase with 110 (27.9°) and 101 (34.6°) crystals. This result indicates that the crystallization of Ta<sub>2</sub>O<sub>5</sub> is affected by IrO<sub>2</sub> component. The intensity of diffraction peaks of IrO<sub>2</sub> appear to increase at high IrO<sub>2</sub> concentration (60%, 70% and 90%), which mean that the aggregation of IrO<sub>2</sub> crystallites with the increase of the content of IrO<sub>2</sub> in the coating. In addition, diffraction peaks corresponding to the Ti support are also observed but no TiO<sub>2</sub> is detected. Ti may come from the penetration of X-ray to reach the substrate in some thin areas and/or the diffusion into the coating from substrate during the thermal preparation<sup>[33]</sup>. SEM observation, together with XRD results indicate that the constitution plays a vital role in determining the surface morphology and structure.

### 3.3 Effect of IrO<sub>2</sub> content on electrocatalytic activity

Cyclic voltammograms of Ti/IrO<sub>2</sub>-Ta<sub>2</sub>O<sub>5</sub> anodes with different content of IrO<sub>2</sub> recorded at a potential scan rates of 20 mV·s<sup>-1</sup> in 0.5 mol·L<sup>-1</sup> H<sub>2</sub>SO<sub>4</sub> solution are shown in Figure 4. The anodes with different IrO<sub>2</sub> contents exhibit a voltammogram typical of the oxide electrodes with a pseudocapacitive behavior, while the electrochemical response is typical of a capacitor exhibiting accurately rectangular mirror images and rapid reversals of directions of response currents. The process of charge and discharge of IrO<sub>2</sub>:  $IrO_a(OH)_b \leftrightarrow IrO_{(a+\delta)}(OH)_{(b-\delta)} + \delta H^+ + \delta e^-$ . When the potential is higher than 0.2V, the occurrence of OH adsorption and further oxidation with oxygen species began. In the cyclic voltammetric curves, the peak at 0.69V (vs. SCE) corresponds to the conversion of Ir(III)/Ir(IV) and the conversion of Ir(IV)/Ir(V)

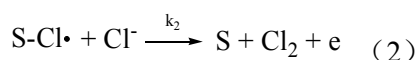
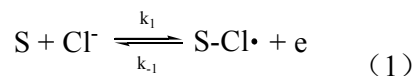
or Ir(IV)/Ir(VI) is 1.0V (vs. SCE)<sup>[30,47,57,59]</sup>. When it comes to Ir(III)/Ir(IV) transformation,  $a=1$ ,  $b=1$ ,  $\delta=1$ ; Ir(IV)/Ir(V) transformation,  $a=1$ ,  $b=2$ ,  $\delta=1$ ; Ir(IV)/Ir(VI) transformation,  $a=1$ ,  $b=2$ ,  $\delta=2$ . The pair of peaks at 0.69V (vs. SCE) has good reversibility, which is concluded from the symmetrical shape of the peaks. This indicates that the surface electrochemistry of the electrode is governed by the active component of IrO<sub>2</sub>.

As shown in Figure 4, it is quite obvious that the voltammetric current of Ti/IrO<sub>2</sub>-Ta<sub>2</sub>O<sub>5</sub> anode with 70 mol% IrO<sub>2</sub> content is greater than that of other anodes. The voltammetric charge capacity ( $q^*$ ) obtained by integration of the cyclic voltammograms indicates the amount of protons exchanged with the solution. Therefore, the value of  $q^*$  is expected to be proportional to the electrochemically active surface area and thought to be able to represent the number of electrochemically active sites on the surface<sup>[30,47,57]</sup>. Figure S1 is the value of  $q^*$  of different content of IrO<sub>2</sub>. The electrochemically active surface area increases gradually as the content of IrO<sub>2</sub> increases at beginning. When the content of IrO<sub>2</sub> reaches to 70%, the sample has the biggest electrochemically active surface area because of its special morphology. And then the electrochemically active surface area of 90% IrO<sub>2</sub> electrode decreases evidently because of the aggregation of IrO<sub>2</sub> crystal particles. So the addition of Ta<sub>2</sub>O<sub>5</sub> can improve the dispersion of iridium oxide grain, and change the electrode morphology, therefore enhance the electrochemically active surface area. From the above discussion, it is evident that the electrochemically active surface area is determined not only by the content of active component, but also by the structure and morphology of the anode coating.

In consideration of the fact that the electrolytic production of chlorine and hypochlorous acid from chloride could be used for food disinfection, the electrocatalytic activity was

investigated by studying the model chlorine evolution reaction (CER). Linear Sweep Voltammetry of Ti/IrO<sub>2</sub>-Ta<sub>2</sub>O<sub>5</sub> anodes with different contents of IrO<sub>2</sub> are shown in Figure 5. The result show that accounting for the intrinsic catalytic activity and morphology<sup>[41,44,51,60,61]</sup>, significant differences still remain among current density at constant electrode overpotential. In agreement with electrochemically active surface area, the current of CER reaches the maximum at the IrO<sub>2</sub> content of 70%. This result verifies that the electrochemically active surface area plays an important role in determining the chlorine evolution.

Furthermore, the mechanism of CER is studied through the Tafel plot. In Figure 6, Tafel curves showed a deviation from linearity at high overpotentials, requiring correction for ohmic drop in order to permit an appropriate interpretation. A single linear segment is obtained showing kinetics of the CER is independent of potential. The Tafel slope is 46.9mV·dec<sup>-1</sup> for 70% IrO<sub>2</sub> electrode, indicating that desorption is the rate-determining step of the reaction (Volmer-Heyrovsky)<sup>[34,47]</sup>. The reaction process is divided into two steps, the second step is the reaction rate controlling step (s represents the active site).



### 3.4 Effect of IrO<sub>2</sub> content on EO water's preparation

The properties of EO water prepared by Ti/IrO<sub>2</sub>-Ta<sub>2</sub>O<sub>5</sub> anodes with different content of IrO<sub>2</sub> are shown in Table 1. The available chlorine content (ACC) and the content of HClO are the very important characteristics in the EO water's preparation<sup>[47,62]</sup>. From Table 1, it is clear that EO water has the maximum value of ACC at the IrO<sub>2</sub> content of 70%, which verifies again that the Ti/IrO<sub>2</sub>-Ta<sub>2</sub>O<sub>5</sub> anode with 70% IrO<sub>2</sub> has the best electrocatalytic activity for chlorine evolution.

It can also be seen from table 1, the higher the chlorine content is, the better sterilization of EO water is. When the IrO<sub>2</sub> content is at 70%, the maximum value of Killing logarithm value and killing rate is 3.05 and 99.9109% respectively. So it is the most suitable content for preparation for EO water. In different forms of chlorine, hypochlorous acid is the main active substance of the sterilization, the sterilization efficiency is 80 times of sodium hypochlorite<sup>[62]</sup>. From the figure 7, the HClO content is a few for 10% IrO<sub>2</sub>, so the killing logarithm value and killing rate are also lower than others. As for 60%, 70% and 90%, the contents of HClO are close, so the sterilization effects are similar. But we can also see that the HClO content is the biggest for 70% IrO<sub>2</sub>, so it has the best bactericidal activity.

### 3.5 Effect of temperature on the surface morphology and electrocatalytic activity

Figure 8 and Figure 9 show the SEM images and X-ray diffraction curves of the Ti/IrO<sub>2</sub>-Ta<sub>2</sub>O<sub>5</sub> anodes with 70% IrO<sub>2</sub> prepared at different temperatures. From Figure 8 and Figure 9, it was observed that the morphology and the surface composition of the electrodes are different when prepared at different temperature. The obvious differences indicate that the temperature has a significant effect on the surface microstructure and the element distribution. At the sintering temperature of 450°C, there is no obvious peak of the oxide components (IrO<sub>2</sub>) in Figure 9. The amorphous phases of IrO<sub>2</sub> were formed due to the incomplete firing of the gel coating. When the sintering temperature increases up to 500°C, the amount of IrO<sub>2</sub> agglomerated particles increases quickly (Figure 8). As can be seen from the XRD patterns, the diffraction peak of IrO<sub>2</sub> is extremely broad and unsymmetrical, which suggests unsatisfactory crystallinity of IrO<sub>2</sub>. When the sintering temperatures rise up to 550°C and 650°C, the amount of IrO<sub>2</sub> agglomerated particles decrease quickly, and cracks begin to increase and deepen, which will greatly reduce

the active area.

Cyclic voltammograms of Ti/IrO<sub>2</sub>-Ta<sub>2</sub>O<sub>5</sub> anodes prepared at different temperatures tested in 0.5 mol·L<sup>-1</sup> H<sub>2</sub>SO<sub>4</sub> solution at a sweeping rate of 20 mV·s<sup>-1</sup> are shown in Figure 10. It can be seen that the sample prepared at 500 °C has the biggest electrochemically active surface area in Figure S2. Then, the electrochemically active surface area decreases evidently with the increase of the sintering temperature. The reduction of the active area should be attributed to the high temperature, which lead to grain growth and aggregation. Secondly, Ta enrichment occurs easily at high temperature, reducing the distribution of IrO<sub>2</sub> active component. This phenomenon can lead to a decrease in the number of active surface sites. In addition, Ti substrate tends to be oxidized at temperatures higher than 500 °C, leading to a decrease in electrode conductivity and a decline in the electrode apparent activity. This result proves again that the electrochemically active surface area is determined by the structure and morphology of the anode coating.

Linear Sweep Voltammetry of Ti/IrO<sub>2</sub>-Ta<sub>2</sub>O<sub>5</sub> anodes prepared at different temperatures tested in saturated sodium chloride solution at a sweeping rate of 20 mV·s<sup>-1</sup> are shown in Figure 11. It can be seen that the current of chlorine evolution also reaches the maximum prepared at 500 °C. This is in line with the above study as shown in Figure 4 and Figure 5.

### 3.6 Effect of temperature on EO water's preparation

The properties of electrolyzed oxidizing water prepared by Ti/IrO<sub>2</sub>-Ta<sub>2</sub>O<sub>5</sub> anodes prepared at different temperature are shown in Table 2. It can be seen that EO water has the maximum value of ACC and HClO prepared at 500 °C, which also proves again the Ti/IrO<sub>2</sub>-Ta<sub>2</sub>O<sub>5</sub> anodes prepared at 500 °C has the best electrocatalytic activity for chlorine evolution. It also can be seen that from table 2, when the preparation temperature is 500 °C, the maximum value of

Killing logarithm value and killing rate is 3.01 and 99.9023% respectively. Therefore, when the temperature is 500 °C, it is most suitable for EO water preparation. In the figure 12, hypochlorous acid content first increased and then decreased with the increase of temperature. We can see that the HClO content is the biggest at 500 °C, which make it has the best of its bactericidal activity.

### 3.7 The accelerated lifetime of Ti/IrO<sub>2</sub>-Ta<sub>2</sub>O<sub>5</sub> anodes

Accelerated lifetime test (ALT) of Ti/IrO<sub>2</sub>-Ta<sub>2</sub>O<sub>5</sub> anodes with different activation time under constant current electrolysis in 0.5mol·L<sup>-1</sup> H<sub>2</sub>SO<sub>4</sub> solution at 2A·cm<sup>-2</sup> is shown in Figure 13. The change of cell voltage with electrolysis time per unit loading during the ALT. The whole period can be divided into three stages: active, stable and deactivate periods. At the beginning, the potential stays at the activation stage, when the electrolyte does not penetrate into the inner surface. After a certain time, it tends to stabilize; this period occupies the main portion of the whole electrolysis time. The potential starts to increase abruptly at the end, and within a short time (less than 15h) the anode is deactivated. As can be seen from Figure 13, the IrO<sub>2</sub>-Ta<sub>2</sub>O<sub>5</sub> coated Ti substrate without activating treatment has the shortest accelerated life (35h). The stability of Ti/IrO<sub>2</sub>-Ta<sub>2</sub>O<sub>5</sub> anode can be improved evidently when Ti substrate was dealt with activating treatment. So the activating treatment for Ti substrate is an effective method in improving the stability of Ti/IrO<sub>2</sub>-Ta<sub>2</sub>O<sub>5</sub> anodes. On the other hand, the Ti/IrO<sub>2</sub>-Ta<sub>2</sub>O<sub>5</sub> anodes differ greatly in terms of anode stability with different activating time. When the activating time increases from 0min to 40min, the anode stability also increases significantly. However, when the activating time comes up to 60min, the anode stability becomes lower. The change in ALT may be attributed to the different structure of Ti substrate. So the surface morphologies of Ti

substrate with different activating time were studied by SEM images shown in Figure S3. Figure S3(a) shows that the Ti substrate has the smooth surface. When activating treatment is used, the surface morphologies become more and more rough. With the increase of the activating time of the Ti substrate, the corrosion pits formed on the surface of Ti substrate gets deeper and deeper. But if the activating time is too long, it would cause excessive corrosion of the substrate surface. Gas can easily go into the electrochemically active sites within the oxide coating, so that it will fall off and electrochemical dissolution occurs, resulting in the consumption of electrochemically active sites, thus the accelerated life will reduce.

#### 4 Conclusions

Through the study of different series of Ti/IrO<sub>2</sub>-Ta<sub>2</sub>O<sub>5</sub> anodes, It can be seen that the preparation conditions has a great impact on the electrode catalytic activity. The influences of IrO<sub>2</sub> content, temperature and activation time on the electrode catalytic activity for Ti/IrO<sub>2</sub>-Ta<sub>2</sub>O<sub>5</sub> anodes were investigated by SEM, XRD, CV, LSV and accelerated lifetime test. The experimental results indicate that that the electrochemically active surface area is determined by the structure and morphology of the anode coating. the IrO<sub>2</sub> aggregated as segregated crystallite particle at the content of 70% prepared at 500°C brings about the best electrode catalytic activity. The properties and sterilization effect of EO water are closely related to the electrode catalytic activity. When the IrO<sub>2</sub> content is 70% and the preparation temperature is 500°C, the maximum value of Killing logarithm value and killing rate is 3.01-3.05 and 99.9023-99.9109% respectively. In addition, when the Ti substrate was dealt with 40 minutes of activation treatment, the Ti/IrO<sub>2</sub>-Ta<sub>2</sub>O<sub>5</sub> anodes has the best stability.

### Author Information

Corresponding Author

\*Z.R.: e-mail, renzhandong@163.com; tel, +86 27 83943956

\*Y.Z.: e-mail, zhuyuchan@163.com; tel, +86 27 83943956

### Acknowledgement

The authors would like to acknowledge financial support from The National Natural Science Foundation of China (31101370) and The Natural Science Foundation of Hubei Province (2012FFB04803).

### References

1. R. M. S. Thorn, S. W. H. Lee, G. M. Robinson, J. Greenman, D. M. *Eur. J. Clin. Microbiol. Infect. Dis.*, 2012, 31:641-653
2. H. C. Zhang, Y. C. Zhu, Z. D. Ren, D. Pan, Y. Liu, Y. R. Wang, B. Cai. *Transactions of the Chinese Society of Agricultural Engineering*, 2013, 29: 277-283
3. L. A . Keskinen, A. Burke, B. A . Annous. *Int. J. Food Microbiol.*, 2009, 132: 134-140
4. S. Koide, D. Shitanda, M. Note, W. Cao. *Food Control*, 2011, 22: 452-456
5. S. McCarthy, W. Burkhardt III. *Food Control*, 2012, 24: 214-219
6. J. Xie, X. H. Sun, Y. J. Pan, Y. Zhao. *Food Control*, 2012, 23: 320-324
7. S.M.E. Rahman, J. Wang, D.-H. Oh. *Food Control*, 2013, 30: 176-183
8. Z. D. Ren, Y. C. Zhu, Y. Liu, Z. Y. Zhang, Q. Zhang. *Transactions of the Chinese Society for Agricultural Machinery*, 2009, 12: 139-143
9. Y. Liu, Z. D. Ren, Z. K. Liu, X. W. Zhang. *Food Science*, 2009, 14: 119-122

10. W. Cao, Z. W. Zhu, Z. X. Shi, C. Y. Wang, B. M. Li. *Int.J. Food Microbiol.*, **2009**, **130**: **88-93**
11. A. Graca, M. Abadias, M. Salazar, C. Nunes. *Postharvest Biol. Tec.*, **2011**, **61**: 172-177
12. K. Xiong, H. J. Liu, L. T. Li. *J. Agric. Food Chem.*, **2012**, **60**: 9770–9778
13. C. Kim, Y. C. Hung, R. E. Brachett. *J. Food Protect.*, **2000**, **63**:19–24(6)
14. L. B. Liao, W. M. Chen, X. M. Xiao. *J. Food Eng.*, **2007**, **78**: 1326–1332
15. S. Koseki, K.Itoh. *J.Food Protect.*, **2001**, **64**: 1935–1942
16. Z. D. Ren, Y. C. Zhu, Y. Liu, X. R. Zhou, Z. Y. Zhang. *Chin. J. Prev. Med.*, **2008**, **8**: **578-581**
17. Z. D. Ren, Y. C. Zhu, Y. Liu, X. R. Zhou, Z. Y. Zhang. *Chinese Journal of Hospital Pharmacy*, **2009**, **17**: 1448-1450
18. Z. D. Ren, Y. C. Zhu, Y. Liu, Z. Y. Zhang. *Journal of Chemical Industry and Engineering*, **2009**, **10**: 2583-2589
19. J. X. Hao, S. Qiu, H. Y. Li, T. P. Chen, H. J. Liu, L. T. Li. *Int. J. Food Microbiol.*, **2012**, **155**: 99– 104
20. H. Kiura, K. Sano, S. Morimatsu, T. Nakano, C. Morita, M. Yamaguchi, T. Maeda, Y. Katsuoka. *J. Microbiol. Meth.*, **2002**, **49**: 285–293
21. Y. R. Huang, Y. C. Hung, S. Y. Hsu, Huang Y. W., Hwang D. F. *Food Control*, **2008**, **19**, **329-345**
22. J. Jeong, J. Y. Kim, J. Yoon. *Environ. Sci. Technol.*, **2006**, **40**: 6117-6122
23. J. X. Hao, S. Qiu, H. Y. Li, T. P. Chen, H. J. Liu, L. T. Li. *Int. J. Food Microbiol.*, **2012**, **155**: 99– 104
24. S. D. Stan, J. S. Woods, M. A. Daeschel. *J. Agric. Food Chem.*, **2005**, **53**: 4901–4905
25. T. Mokudai, K. Nakamura, T. Kanno, Y. Niwano. *Plos One*, **2012**, **9**: e46392
26. S. Y. Hsu. *J. Food Eng.*, **2003**, **60**:469–473.
27. S. Y. Hsu. *J. Food Eng.*, **2005**, **66**: 171-173.

28. X. P. Zeng, M. Zhang, X. D. Wang, X. Y. Chen, X. Z. Su, W. W. Tang. *J. Electroanal. Chem.*, **2012**, **677–680**: 133–138
29. S. Neodoa, D. Rosestolato, S. Ferro, A. D. Battisti. *Electrochim. Acta*, **2012**, **80**: 282-291
30. L. K. Xu, Y. L. Xin, J. T. Wang. *Electrochim. Acta*, **2009**, **54**:1820-1825
31. K. S. Exner, J. Anton, T. Jacob, H. Over. *Angew. Chem. Int. Ed.*, **2014**, **53**: 1-5
32. N. Menzel, E. Ortel, K. Mette, R. Kraehnert, P. Strasser. *ACS Catal.*, **2013**, **3**: 1324–1333
33. Y. Zeng, K. N. Chen, W. Wu, J. R. Wang, S. Lee. *Ceramics International*, **2007**, **33**: 1087-1091
34. M. H. P. Santana, L. A. D. Faria. *Electrochim. Acta*, **2006**, **51**: 3578-3585
35. A. R. Zeradjanin, N. Menzel, W. Schuhmann, P. Strasser. *Phys. Chem. Chem. Phys.*, **2014**, **16**: 13741-13747
36. I. Katsounaros, S. Cherevko, A. R. Zeradjanin, K. J. J. Mayrhofer. *Angew. Chem. Int. Ed.*, **2014**, **53**: 102-121
37. A. R. Zeradjanin, A. A. Topalova, Q. V. Overmeereb, S. Cherevkoa, X. X. Chen, E. Ventosac, W. Schuhmann, K. J. J. Mayrhofer. *RSC Adv.*, **2014**, **4**: 9579
38. V. Petrykin, K. Macounova, O. A. Shlyakhtin, and P. Krtil. *Angew. Chem.*, **2010**, **122**: 4923-4925
39. V. Petrykin, K. Macounova, J. Franc, O. Shlyakhtin, M. Klementova, S. Mukerjee, and P. Krti. *Chem. Mater.*, **2011**, **23**: 200-207
40. T. Reier, M. Oezaslan, and P. Strasser. *ACS Catal.*, **2012**, **2**: 1765-1772
41. R. Y. Chen, V. Trieu, A. R. Zeradjanin, H. Natter, D. Teschner, J. Kintrup, A. Bulan, W. Schuhmann and R. Hempelmann. *Phys. Chem. Chem. Phys.*, **2012**, **14**: 7392-7399
42. S. Y. Chen, Y. H. Zheng, S. W. Wang, X. M. Chen. *Chem. Eng. J.*, **2011**, **172**: 47-51
43. V. Petrykin, K. Macounová, M. Okube, S. Mukerjee, P. Krtil. *Catal. Today*, **2013**, **22**: 63-69
44. V. Trieu, B. Schley, H. Natter, J. Kintrup, A. Bulan, R. Hempelmann. *Electrochim. Acta*, **2012**, **78**: 188-194

45. J. Jirkovský, H. Hoffmannová, M. Klementová, P. Krtil. *J. Electrochem. Soc.*, **2006**, **153**: **E111-E118**
46. N. W. Fan, Z. K. Li, L. Zhao, N. M. Wu, T. Zhou. *Chem. Eng. J.*, **2013**, **214**: **83-90**
47. X. L. Zhou, Z. G. Ye, X. Z. Hua, A. H. Zou, Y. H. Dong. *J. Solid State Electrochem.*, **2010**, **14**: **1213–1219**
48. L. Vazquez-Gomez, S. Ferro, A. De Battisti. *Appl. Catal. B-Environ.*, **2006**, **67**: **34-40**
49. P. Lakshminathiraj, G. B. Raju, Y. Sakai, Y. Takuma, A. Yamasaki, S. Kato, T. Kojima. *Chem. Eng. J.* **2012**, **198-199**: **211-218**
50. B. Johnson, F. Girgsdies, G. Weinberg, D. Rosenthal, A. Knop-Gericke, and R. Schlögl. *J. Phys. Chem. C*, **2013**, **117**: **25443-25450**
51. E. Ortel, T. Reier, P. Strasser, and R. Kraehnert. *Chem. Mater.*, **2011**, **23**: **3201-3209**
52. R. Tolba, M. Tian, J. L. Wen, Z. H. Jiang, A. C. Chen. *J. Electroanal. Chem.*, **2010**, **649**: **9-15**
53. K. C. Pillai, T. O. Kwon, B. B. Park, I. S. Moon. *J. Hazard. Mater.*, **2009**, **164**: **812-819**
54. T. L. Luu, J. Y. Kim, J. Y. Yoon. *J. Ind. and Eng. Chem.*, **2014**, **in press**
55. L.K. Xu, J.D. Scantlebury. *Corrosion Science*. **2003**, **45**: **2729-2740**
56. J.M. Hu, H.M. Meng, J.Q. Zhang, C.N. Cao. *Corrosion Science*. **2002**, **44**: **1655-1668**
57. Z. W. Yan, H. M. Meng. *Rare Metals*, **2011**, **30(5)**: **439-446**
58. Carrell Morris J. *J. Phy. Chem.*, **1966**, **70(12)**: **3798-3805**.
59. S. Ardizzone, C.L. Bianchi, G. Cappelletti, M. Ionita, A. Minguzzi, S. Rondinini, A. Vertova. *J. Electroanal. Chem.*, **2006**, **589**: **160–166**
60. A. R. Zeradjanin, F. L. Mantiab, J. Masaa, W. Schuhmann. *Electrochim. Acta*, **2012**, **82**: **408-414**
61. H. Z. Cao, D. H. Lu, J. P. Lin, Q. Ye, J. J. Wu, G. Q. Zheng. *Electrochim. Acta*, **2013**, **91**: **234-239**

62. Kim, C.; Hung, Y. C.; Brackett, R. E. *Int. J. Food Microbiol.*, 2000, 61, 199-207.

## Figure captions

**Fig.1** A schematic representation of the electrolyzed oxidizing preparation, detection and sterilization

**Fig.2** SEM images for Ti/IrO<sub>2</sub>-Ta<sub>2</sub>O<sub>5</sub> anodes with (a) 10% IrO<sub>2</sub>, (b) 40% IrO<sub>2</sub>, (c) 60% IrO<sub>2</sub>, (d) 70% IrO<sub>2</sub>, (e) 90% IrO<sub>2</sub>, (f) a cross-section of 70% IrO<sub>2</sub>

**Fig.3** X-ray diffraction curves for Ti/IrO<sub>2</sub>-Ta<sub>2</sub>O<sub>5</sub> anodes with (a) 10% IrO<sub>2</sub>, (b) 40% IrO<sub>2</sub>, (c) 60% IrO<sub>2</sub>, (d) 70% IrO<sub>2</sub>, (e) 90% IrO<sub>2</sub>

**Fig.4** Cyclic voltammograms of Ti/IrO<sub>2</sub>-Ta<sub>2</sub>O<sub>5</sub> anodes with different contents of IrO<sub>2</sub> in 0.5mol·L<sup>-1</sup> H<sub>2</sub>SO<sub>4</sub> solution at a sweeping rate of 20mV·s<sup>-1</sup>

**Fig.5** Linear Sweep Voltammetry of Ti/IrO<sub>2</sub>-Ta<sub>2</sub>O<sub>5</sub> anodes with different contents of IrO<sub>2</sub> in saturated sodium chloride solution at a sweeping rate of 20mV·s<sup>-1</sup>

**Fig.6** Tafel plot curve of Ti/IrO<sub>2</sub>-Ta<sub>2</sub>O<sub>5</sub> with 70% IrO<sub>2</sub> and 500°C

**Fig.7** The absorbance of HClO of Ti/IrO<sub>2</sub>-Ta<sub>2</sub>O<sub>5</sub> anodes with different contents of IrO<sub>2</sub> at 233nm

**Fig.8** SEM images for Ti/IrO<sub>2</sub>-Ta<sub>2</sub>O<sub>5</sub> anodes with 70% IrO<sub>2</sub> prepared at different temperature (a) 450°C, (b) 500°C, (c) 550°C, (d) 650°C

**Fig.9** X-ray diffraction curves for Ti/IrO<sub>2</sub>-Ta<sub>2</sub>O<sub>5</sub> anodes with 70% IrO<sub>2</sub> prepared at different temperature (a) 450°C, (b) 500°C, (c) 550°C, (d) 650°C

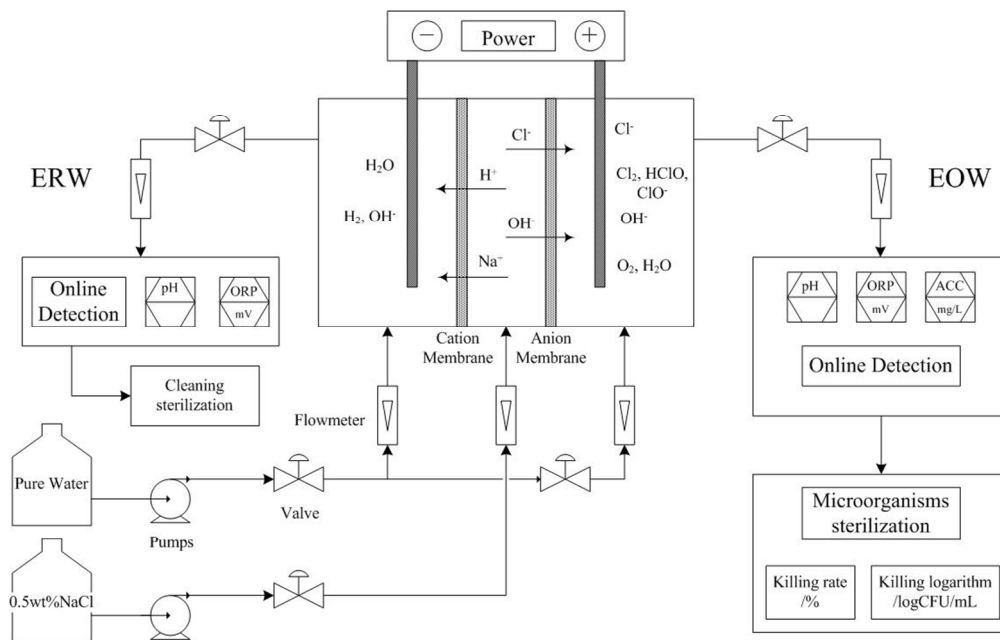
**Fig.10** Cyclic voltammograms of Ti/IrO<sub>2</sub>-Ta<sub>2</sub>O<sub>5</sub> anodes with 70% IrO<sub>2</sub> prepared at different temperatures tested in 0.5mol·L<sup>-1</sup> H<sub>2</sub>SO<sub>4</sub> solution at a sweeping rate of 20mV·s<sup>-1</sup>

**Fig.11** Linear Sweep Voltammetry of Ti/IrO<sub>2</sub>-Ta<sub>2</sub>O<sub>5</sub> anodes prepared at different temperatures tested in saturated sodium chloride solution at a sweeping rate of 20mV·s<sup>-1</sup>

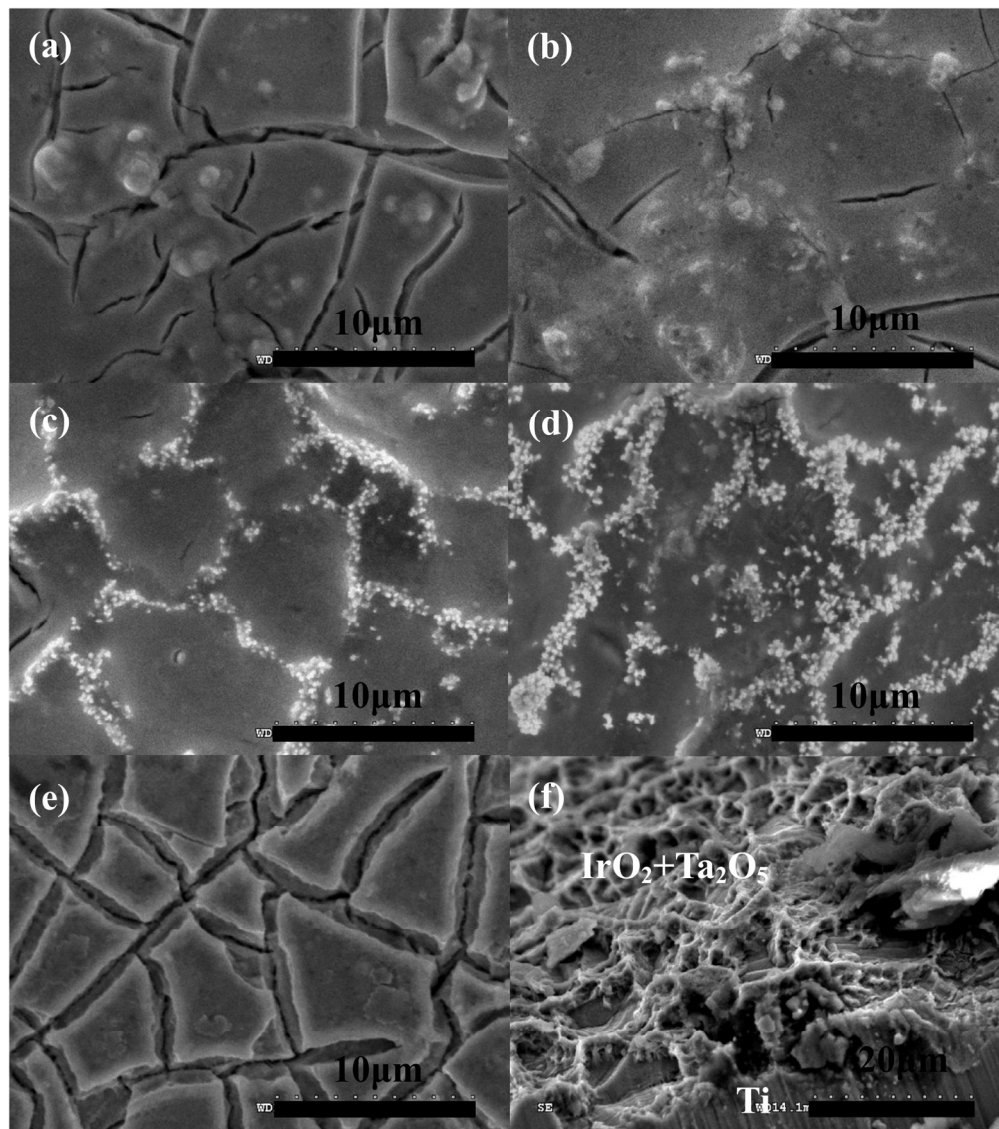
**Fig.12** The absorbance of HClO of Ti/IrO<sub>2</sub>-Ta<sub>2</sub>O<sub>5</sub> anodes with different temperatures

at 233nm

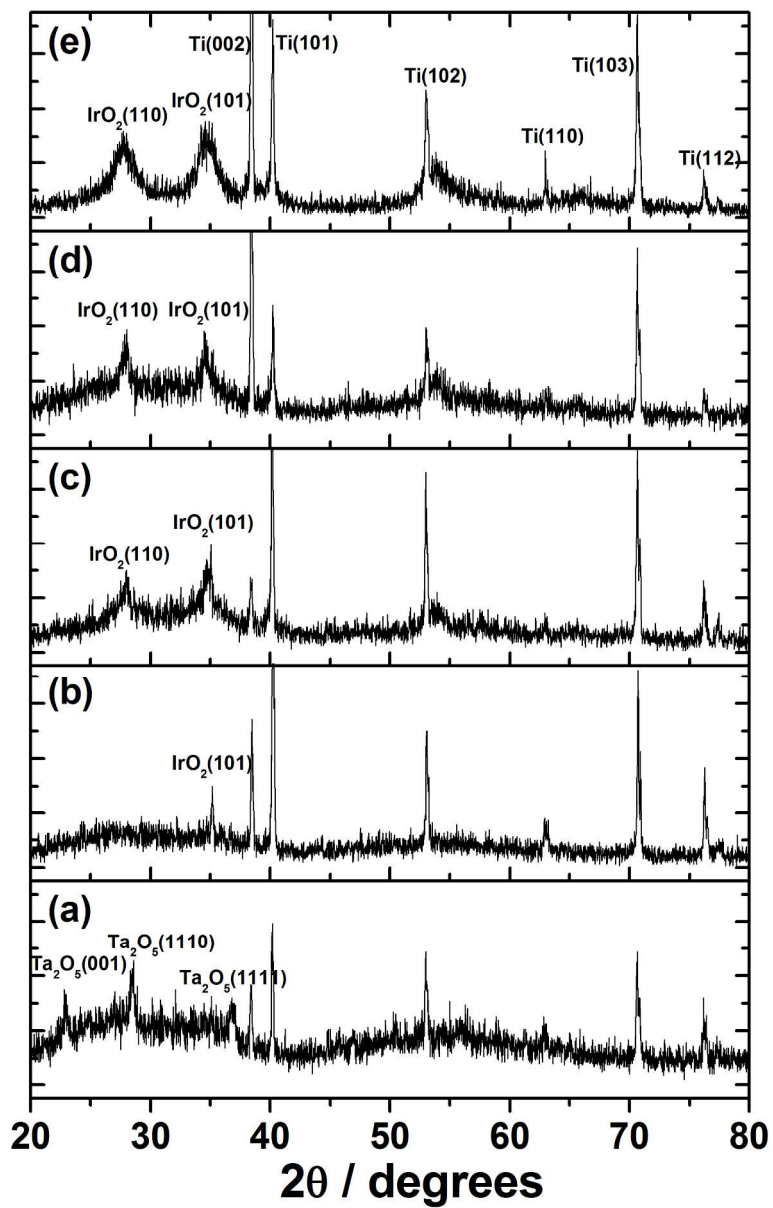
**Fig.13** Accelerated lifetime of Ti/IrO<sub>2</sub>-Ta<sub>2</sub>O<sub>5</sub> anodes with different activation time under constant current electrolysis in 0.5 mol·L<sup>-1</sup> H<sub>2</sub>SO<sub>4</sub> solution at 2A·cm<sup>-2</sup>



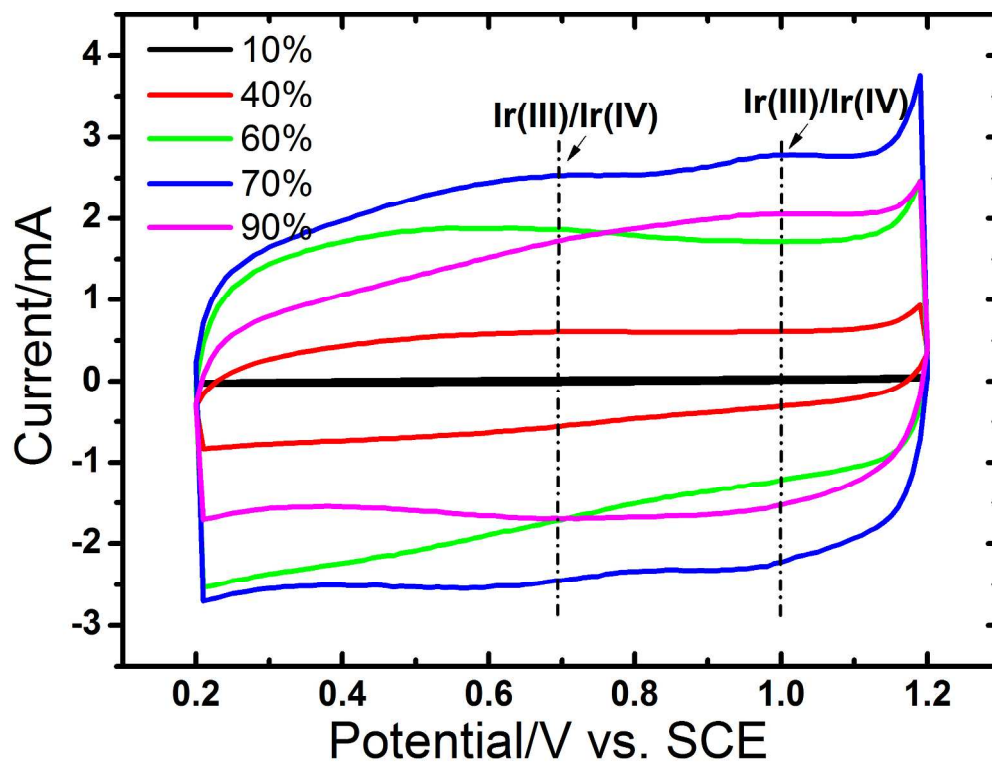
304x192mm (96 x 96 DPI)



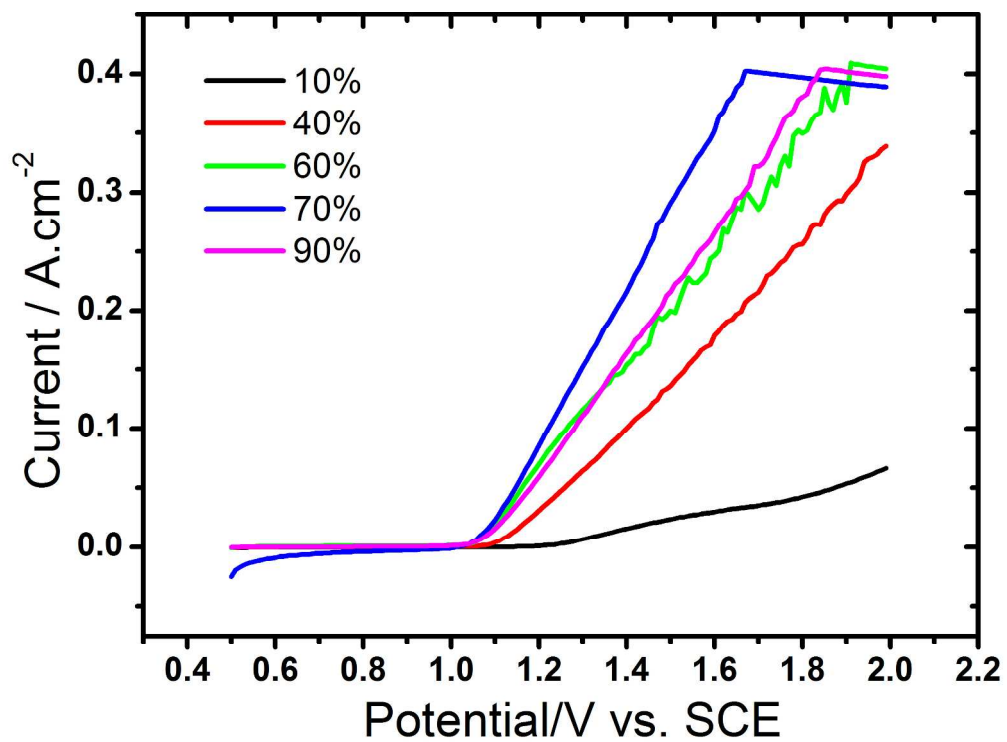
490x551mm (96 x 96 DPI)



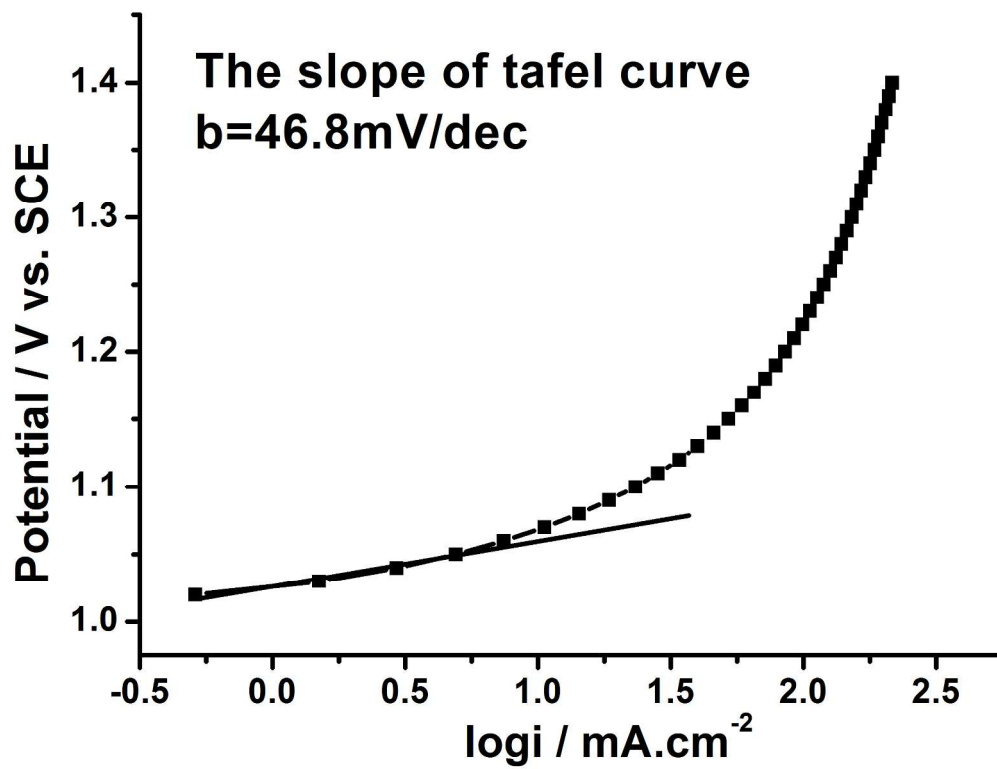
168x262mm (300 x 300 DPI)



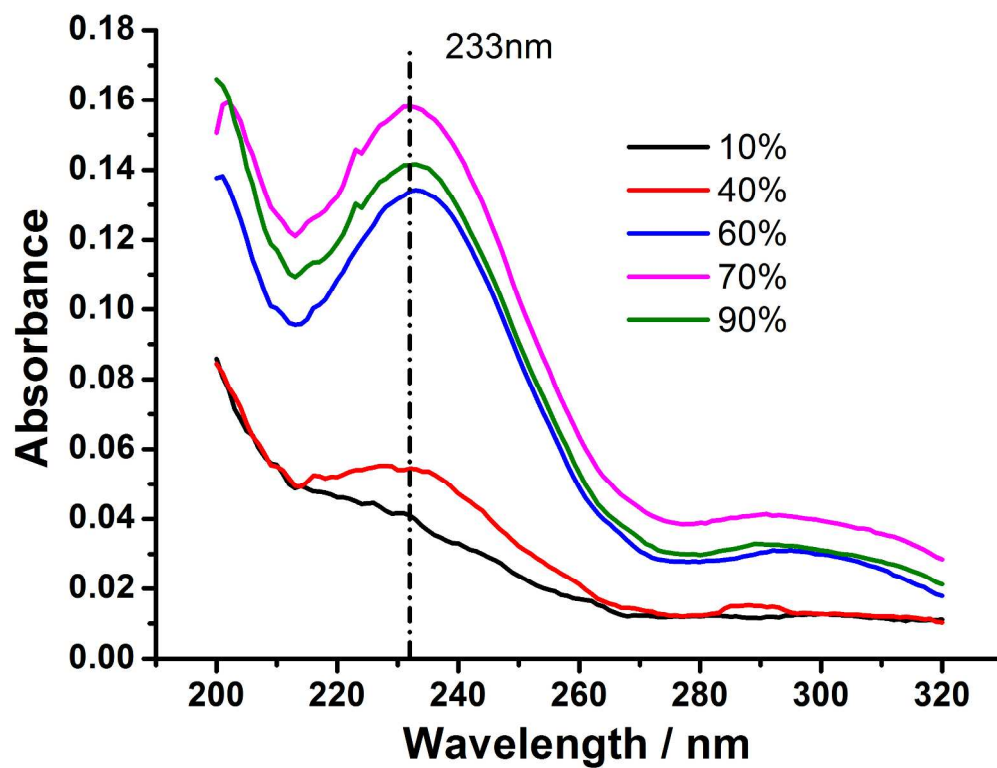
231x175mm (300 x 300 DPI)



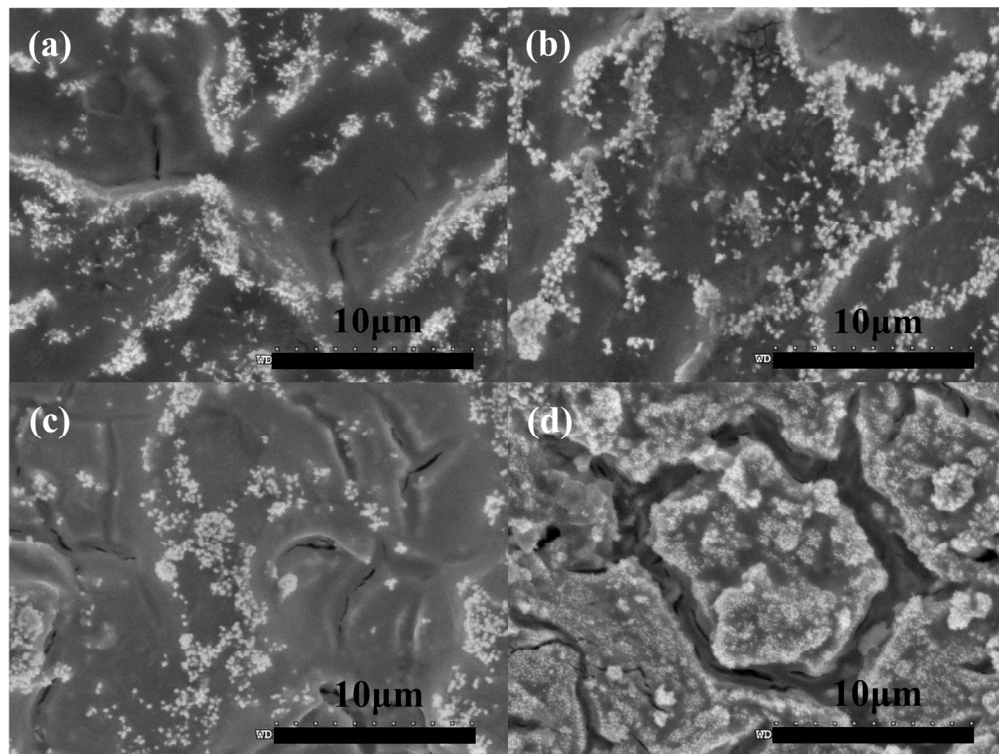
243x178mm (300 x 300 DPI)



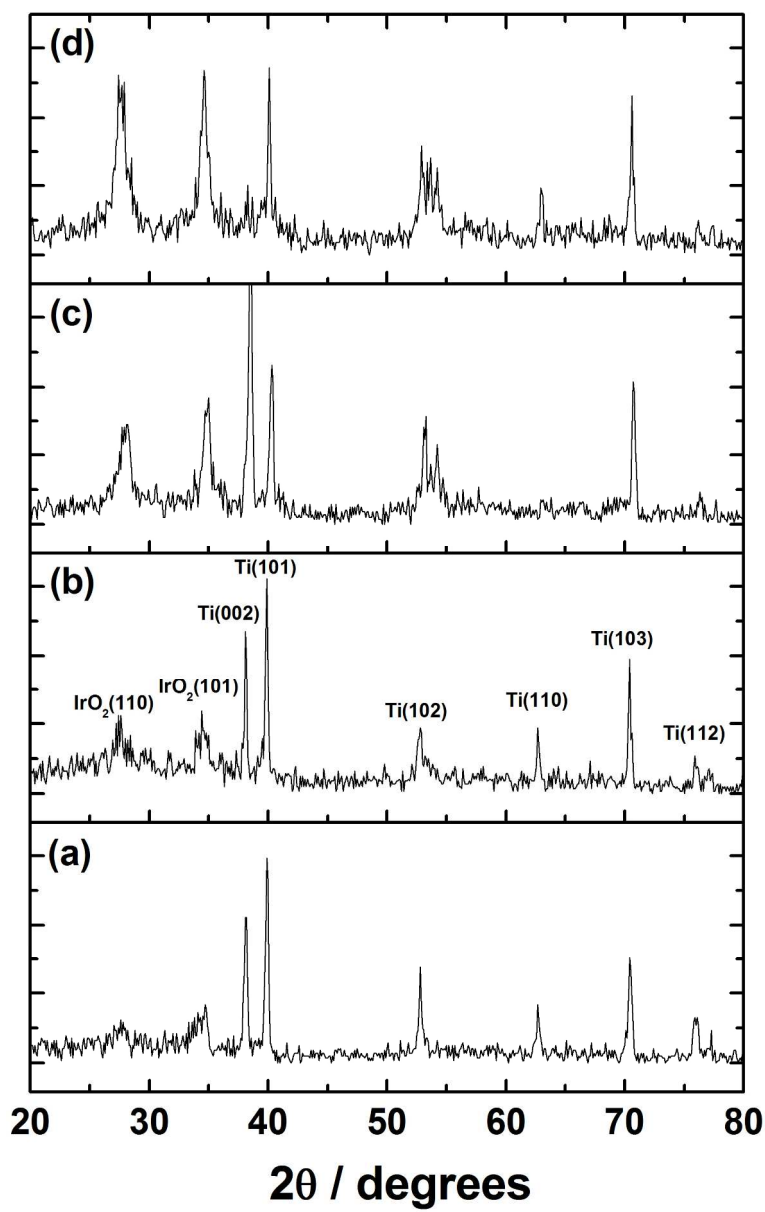
235x178mm (300 x 300 DPI)



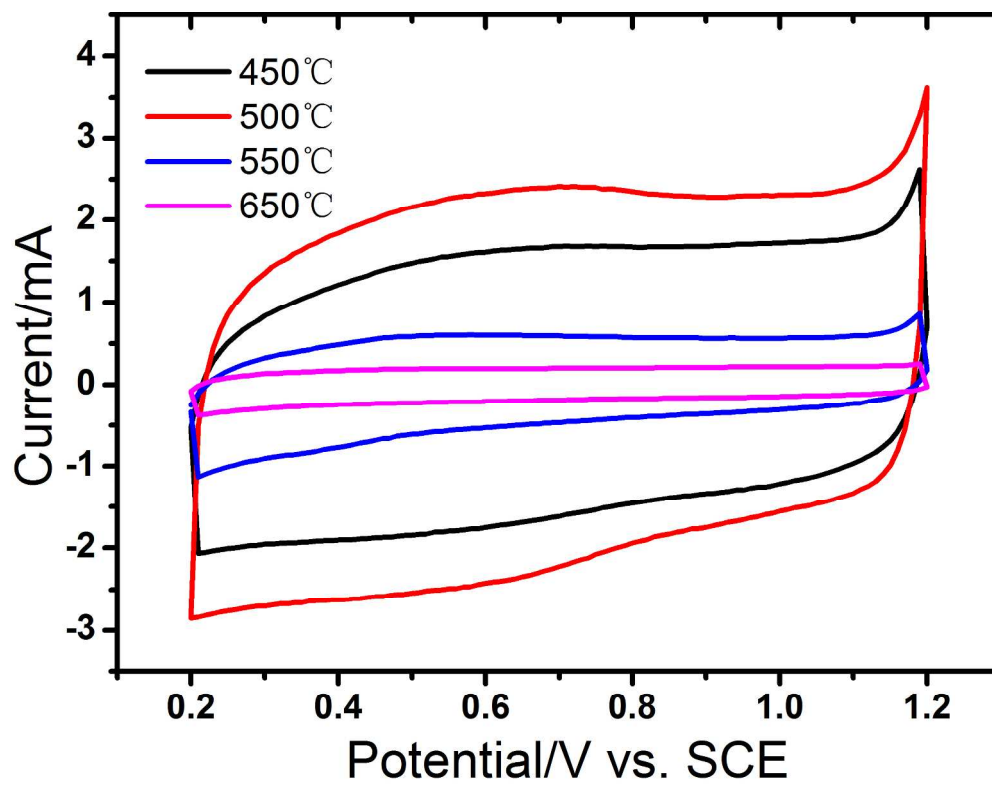
239x183mm (300 x 300 DPI)



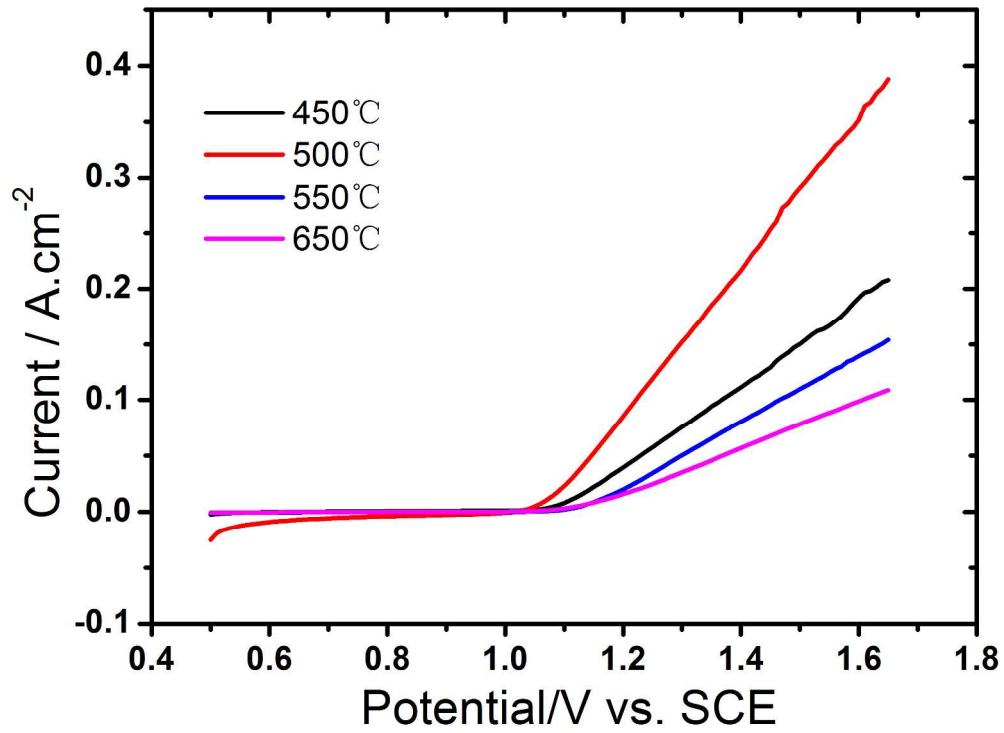
490x367mm (96 x 96 DPI)



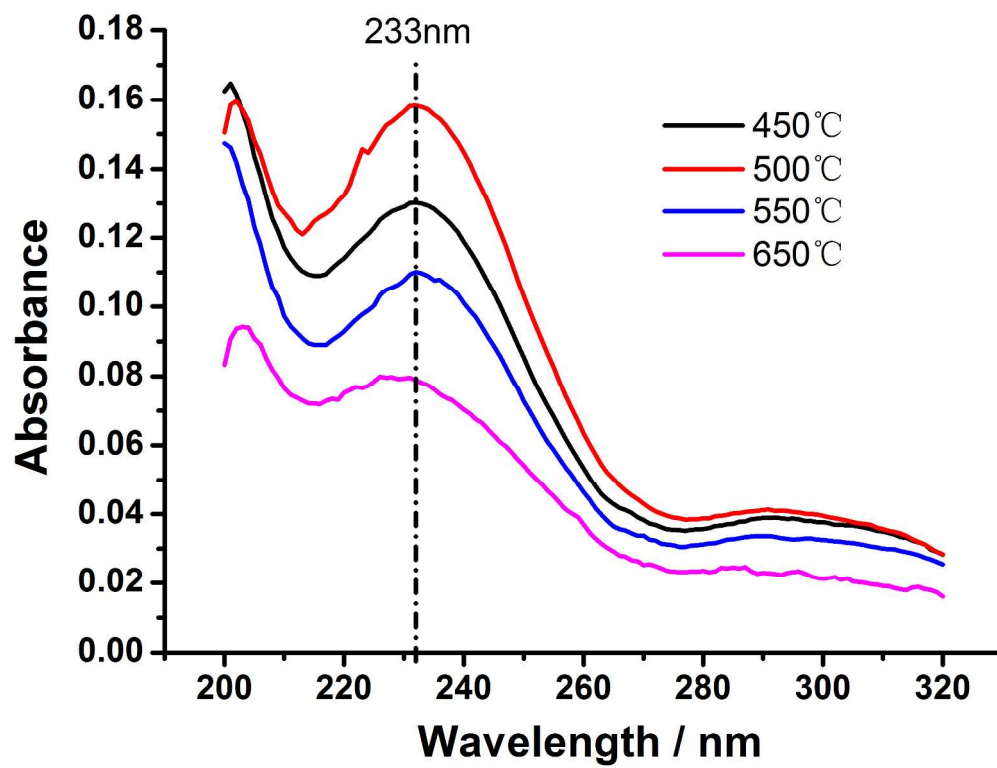
168x264mm (300 x 300 DPI)



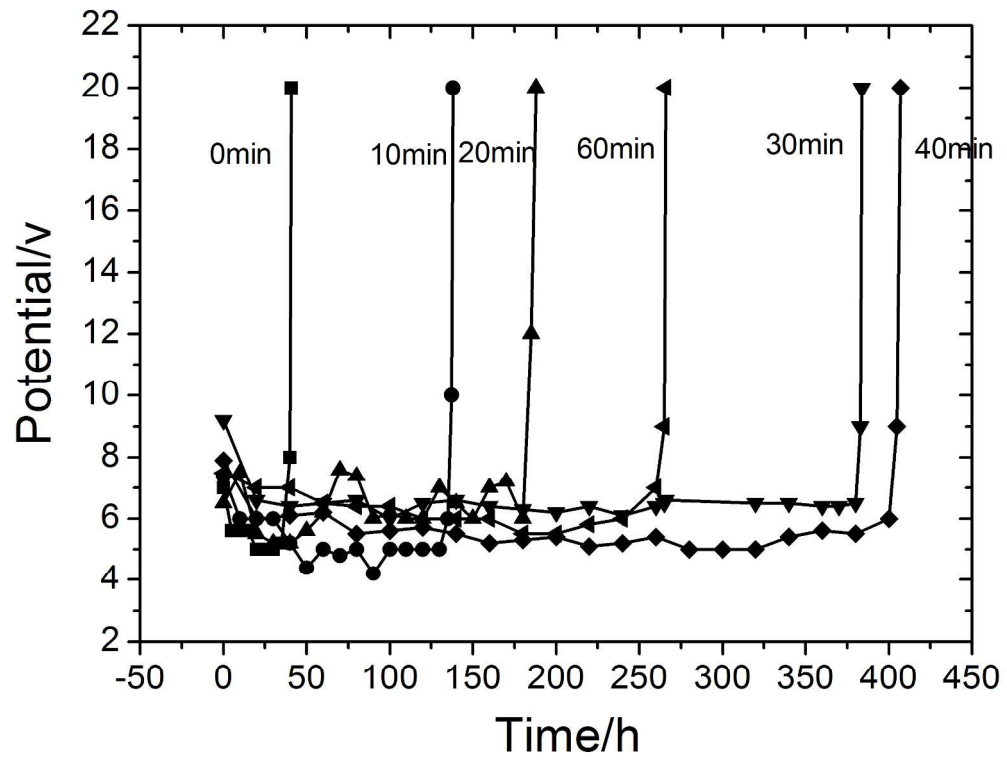
229x178mm (300 x 300 DPI)



245x178mm (300 x 300 DPI)



242x185mm (300 x 300 DPI)



243x187mm (300 x 300 DPI)

**Table 1** The sterilization effect and EO water's physicochemical property depending on the IrO<sub>2</sub> content of Ti/IrO<sub>2</sub>-Ta<sub>2</sub>O<sub>5</sub> anodes

Content /mol%	Physicochemical property			Sterilization effect	
	pH	ORP /mV	ACC /mg·L <sup>-1</sup>	Killing logarithm value / logCFU·mL <sup>-1</sup> ⊙	Killing rate /%⊙
10	2.24	1146	31.64	2.30	99.4988
40	2.24	1149	69.83	2.76	99.8682
60	2.24	1152	85.66	2.92	99.8798
70	2.20	1150	90.17	3.05	99.9109
90	2.17	1150	83.56	2.90	99.8741

Note: ⊙Positive control group (*Bacillus subtilis var. niger*): 7.53 logCFU/mL, killing time: 30min.

**Table 2** The sterilization effect and EO water's physicochemical property depending on the preparation temperature of Ti/IrO<sub>2</sub>-Ta<sub>2</sub>O<sub>5</sub> anodes

temperature /°C	Physicochemical property			Sterilization effect	
	pH	ORP /mV	ACC /mg·L <sup>-1</sup>	Killing logarithm value / logCFU·mL <sup>-1</sup> ⊙	Killing rate /%⊙
450	2.24	1146	83.51	2.71	99.8050
500	2.29	1150	90.17	3.01	99.9023
550	2.30	1141	83.96	2.90	99.8741
650	2.27	1146	66.22	2.88	99.8682

Note: ⊙Positive control group (*Bacillus subtilis var. niger*): 7.53 logCFU/mL, killing time: 30min.